Spectroscopy of Hydrothermal Reactions. 10. Evidence of Wall Effects in Decarboxylation Kinetics of 1.00 *m* HCO_2X (X = H, Na) at 280−330 °C and 275 bar

P. G. Maiella and T. B. Brill*

Department of Chemistry and Biochemistry, University of Delaware, Newark, Delaware 19716

Received: February 17, 1998; In Final Form: May 11, 1998

Decomposition kinetics of 1.00 *m* formic acid and sodium formate to form CO_2 (and H_2) were probed under hydrothermal conditions of 280−330 °C and 275 bar. Flow reactor spectroscopy cells constructed from different metals (316 stainless steel, 90/10 Pt/Ir alloy, and grade 2 Ti) with diamond and sapphire windows were used to determine the rate of formation of CO_2 in situ by IR spectroscopy. A single fluid phase was maintained. CO_2 was produced at different rates depending on the metal and, in the case of 316 stainless steel, with a lot-dependent, concentration−time profile. The values of $E_a = 87-121$ kJ/mol resemble those previously reported for surface- and H_2O-catalyzed decarboxylation of formic acid. Much higher E_a values are reported for unimolecular decomposition. Sodium formate decarboxylates more slowly than formic acid. In contrast to formic acid, the rate of decarboxylation of malonic acid in all of the cells is the same within error, which is consistent with a homogeneous unimolecular reaction.

Introduction

Formic acid, HCO_2H, is the simplest carboxylic acid and, as such, is regarded to be fundamentally important as an intermediate in the oxidation of various hydrocarbons.[1−4] Recent interest has also focused on the possible role of HCO_2H as an intermediate in the water-gas shift reaction in supercritical water[5−10] and as a component in wet-air oxidation.[11] As an example of a simple carboxylic acid, HCO_2H has been widely employed in prototypical studies of the formation and stability of intermediates on clean metal and metal oxide surfaces and for comparing the catalytic behavior of materials.[12−18] These latter studies may also be pertinent to the corrosion of stainless steel by formic acid.[19,20]

The decomposition pathways 1−3 have been indicated for HCO_2H:[12,13]

$$HCO_2H \rightarrow CO_2 + H_2 \quad (1)$$

$$\rightarrow CO + H_2O \quad (2)$$

$$\rightarrow {}^1/_2CO_2 + {}^1/_2H_2CO + {}^1/_2H_2O \quad (3)$$

Reactions 1 and 2 are surface-catalyzed in ratios that depend on the substrate, whereas reaction 3 does not occur on a metal surface. The Arrhenius activation energy for first-order decomposition of HCO_2H by reactions 1 and 2 on clean Ni surfaces is 100−109 kJ/mol,[14,21] with $A = 10^{15}$ s^{-1}.[17] This range of E_a values resembles $E_a = 105-113$ kJ/mol[22] for HCO_2H with 1% H_2O and $E_a = 86$ kJ/mol for 0.022 *m* HCO_2H at 320−420 °C in a C-276 Hastelloy tube reactor.[23] Reactions 1 and 2 also are indicated to be decomposition pathways in the gas phase.[24−31] For example, the rate constant for the first-order decarboxylation reaction 1 is $10^{12.47}\exp(-203/(RT))$ s^{-1}, while dehydration by reaction 2 was second order below 600 °C with a rate constant of $10^{11.44}\exp(-133/(RT))$ cm^3 mol^{-1} s^{-1} and 1.5 order above 670 °C with $k = 10^{15.39}\exp(-253/(RT))$ s^{-1} (E_a is in units of kJ/mol).[25] Reaction 2 was reported to have $E_a = 258-280$ kJ/mol in another study.[31] Shock-tube kinetics at still higher temperatures are available.[26,30] Reaction 1 was found to have second-order rate behavior with $E_a = 272-284$ kJ/mol,[30] whereas reaction 2 had $E_a = 259-272$[30] or 169 kJ/mol.[26] These reactions have also been analyzed quantum mechanically,[8,26−29,32] and it is found that eq 1 has a higher activation energy (range = 272−372 kJ/mol; average = 304 kJ/mol) than eq 2 (range = 259−284 kJ/mol; average = 276 kJ/mol). Consistent with early experimental data,[22] the inclusion of H_2O in the transition state lowers the activation energy of reaction 1 substantially.[8,27] One H_2O lowers the E_a of reaction 1 to 157,[8] 200 kJ/mol,[32] or 204 kJ/mol,[27] whereas two H_2O molecules lowers E_a to 90 kJ/mol[8] or 189 kJ/mol.[32] Therefore, computational and experimental evidence reveals that the presence of H_2O and/or a metal surface substantially lowers the E_a of reaction 1 compared to the unimolecular decomposition pathway.

Direct spectral observations of the species during hydrothermolysis of HCO_2H at high pressure and temperature had not been reported when this work began.[33] Such studies should provide more insight into the homogeneous pathway or a surface-mediated pathway when a single-phase solution is present. The unusual CO_2 formation profile observed in a 316 stainless steel (SS) cell[33] suggested that the reactor surface may influence the rate. Design features of the reactor could, therefore, be important in the kinetics obtained for formic acid. If competition exists between the homogeneous and wall-mediated processes, then a large variation in the surface-to-volume ratio (*S*/*V*) should shift the balance of these two general processes. In addition, the role of surface catalysis should be detectable by changing the materials used in the construction of the cell. In the present study a large *S*/*V* reactor with a spectroscopically accessible zone[34,35] was used, and the reaction was observed in real time by transmission IR spectroscopy through a thin sheet of solution. It is experimentally impractical to vary *S*/*V* within our cell, but the material of construction can be changed while maintaining the same cell design. To this

* Corresponding author. E-mail: brill@udel.edu.

S1089-5639(98)01165-7 CCC: $15.00
Published on Web 06/19/1998

end, cells were constructed of SS, Ti, and Pt/Ir alloy containing sapphire and diamond windows. Unlike experiences with amines[36,37] and other carboxylic acids,[37,38] the formation rate of CO_2 from HCO_2H depended significantly on the cell wall composition, which suggests that heterogeneous reactions can be important, especially at high *S*/*V* values. Such details may be important in interpreting and understanding practical hydrothermal reactions, such as occur in geochemical events,[39,40] biomass conversion,[41,42] and waste-stream remediation.[43,44]

Experimental Section

The kinetic experiments were conducted with spectroscopy cells constructed from four types of metals: 90/10 Pt/Ir with diamond windows,[35] types 304 and 316 stainless steel with sapphire windows,[34] and grade 2 titanium with sapphire windows. The precise characteristics of the metal surface in these cells are difficult to specify and could even be viewed as another variable. The SS and Ti cells are expected to have mostly a metal oxide surface. The design of the cells is the same in terms of the flow pattern and was made by the same machinist. *S*/*V* is 20−50 cm^{-1}. The Ti cell was constructed with fittings rather than Ti−Ti welded joints because it was found that aqueous CO_2 rapidly corroded the welded spots, causing poor flushing and eventual leaking. This was true even when care was taken to eliminate O_2 during the welding process. In each case the cell is designed for transmission IR spectroscopy in which the path length is controlled by a gold-foil spacer having a thickness of 30 ± 5 μm. The exact path length in each case was determined from the interference fringe spacing in the IR spectrum.[34,35] The heat transfer and fluid mechanics characteristics of these cells have been modeled,[35] and the flow controls are described elsewhere.[34,35] Plug−flow conditions exist at higher flow rates (lower degree of conversion); however, laminar flow is a better description at low flow rates (higher degree of conversion). As a result of the desire to assume plug−flow, the degree of conversion studied was 40% or less.

The flow rate was controlled by a pulseless, dual-piston, LDC-Analytical HPLC pump or an Isco syringe pump. The results of experiments with two different pumps were the same, indicating that pump characteristics are not a factor in the kinetic data. Five electrical cartridge heaters inserted concentrically in the cell body were used to heat the cell to a temperature that is controlled at ±1 °C and monitored by Omega PID units attached to 0.8 mm K-type thermocouples near the flow path. The pressure was maintained at 275 ± 1 bar by using an air-actuated bleed-and-lock system. The pressure was actively monitored with an Omega melt-pressure transducer. Software written in Visual Basic controlled and recorded the temperature, pressure, and flow rate. Spectra were taken only after the system had stabilized at the desired conditions.

A 1.00 molal (*m*, moles/kg) solution of formic acid (Sigma Chemical Company, 99%) was prepared using HPLC-grade water that had been sparged with Ar to remove atmospheric gases. Sodium formate solutions (1.00 *m*) were made by adding 1 equiv of NaOH. The hydrothermolysis reaction was studied between 280 and 330 °C using 10−40 flow rates at each temperature depending upon the cell and pump employed. Residence times in the range 2.5−20.6 s in the SS cells, 0.8−7.0 s in the Pt/Ir cell, and 4.8−71.4 s in the Ti cell existed after correcting for the change in density of the solution with temperature (i.e., multiply by ρ_o/ρ_T). Spectra were collected using a Nicolet 60SX FTIR spectrometer equipped with a MCT-B detector. The resolution was 4 cm^{-1} with 32 interferrograms being summed at each condition. Each spectrum was then ratioed against a spectrum of pure water at the same conditions. Figure 1 shows a series of IR spectra recorded with the Pt/Ir diamond cell. The interference fringes are apparent in the higher energy region and provide an accurate measurement of the path length of the cell (vide supra). The CO_2 absorbance was followed and, by the absence of gas-phase features, a single (liquid) phase existed at all conditions. Postreaction examination of the cells, even after use for extended periods, did not reveal evidence of corrosion except in the case of 304 SS. Only a slight discoloration of the surface occurred in the other cells.

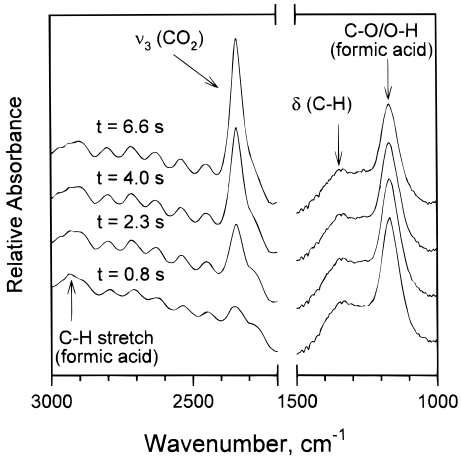

Figure 1. Mid-IR spectra of 1.00 *m* HCO_2H in the Pt/Ir diamond flow cell at 330 °C under 275 bar as a function of the residence time.

Conversion of the ν_3 (CO_2) absorbance areas into concentrations at hydrothermal conditions required the use of calibration data based on the Lambert−Beer law.[34,35] The band area of ν_3 (CO_2) was obtained by fitting each spectrum with a four-parameter Voigt function (Peakfit, Jandel Scientific). A program written in Visual Basic was used to remove the interference fringe pattern. Multiple data sets were collected to determine the error in the rate constant *k*. A weighted least-squares regression was then performed where the statistical weight, ω_i, used was $1/\sigma^2$, where σ is the standard deviation of the concentration values at each time *i*. Where necessary, ω_i was approximated as $k^2\omega_i'$.[46] In a first-order rate constant and Arrhenius analysis, the error limits were translated into log space as $\sigma/\bar{x}$, where $\bar{x}$ is the average CO_2 concentration.[46]

Results and Discussion

The decomposition rate of HCO_2H by reaction 1 is apparent in all of the vibrational modes in the IR spectrum (Figure 1). Several modes are, however, more useful than others. The C−H stretch of HCO_2H (2940 cm^{-1}) could be used, but its low intensity produces considerable uncertainty in the concentration. The decrease in the intensity of the predominantly C−O stretch/O−H bending mode[47] centered at 1175 cm^{-1} could be followed in the Pt/Ir cell but was not used because it is outside the IR band-pass of the sapphire windows used in the other cells. The most useful mode is ν_3 [CO_2(aq)] at 2343 cm^{-1} because we have considerable experience with the line shape and absorbance−concentration relation in the hydrothermal medium,[34,45] and it can be seen with all of the cells. There is no experimental evidence for reaction 2 in part because, unlike in the gas phase, this reaction is less important than reaction 1 in H_2O[11] and in part because the IR absorbance of CO is 0.047 times that of ν_3(CO_2). Likewise, reaction 3 seems unlikely by the absence of the CH_2 bending absorbance of CH_2O at about 1500 cm^{-1}.

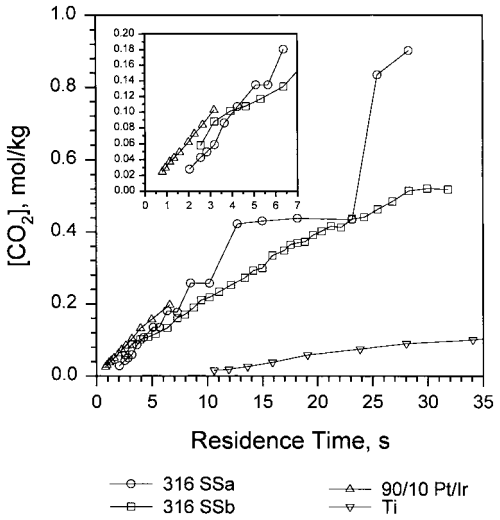

Figure 2. Concentration of CO_2 from 1.00 *m* HCO_2H at 310 °C and 275 bar as a function of residence time in four different cell materials.

On the other hand, CO_2 is produced by two reactions (5 and 6) in the hydrothermal medium because of the equilibrium reaction 4:

$$HCO_2H \rightleftharpoons HCO_2^- + H^+ \quad (4)$$

$$HCO_2H \xrightarrow{k_1} CO_2 + H_2 \quad (5)$$

$$HCO_2^- + H_2O \xrightarrow{k_2} CO_2 + H_2 + OH^- \quad (6)$$

Consequently, as will be discussed later, decarboxylation of HCO_2H in H_2O necessitates consideration of the kinetics from both the HCO_2H and HCO_2^- sources.

A central feature of this work is the observation that the rate of formation of CO_2 depends on the material used to construct the cell. The gold foil used as a spacer in every cell is not a variable. The diamond and sapphire windows are neither catalytic nor a variable. On the other hand, the cell body, which was made from two grades of SS, 90/10 Pt/Ir alloy, and grade 2 Ti, is a major variable. Figure 2 shows the rate of formation of CO_2 from 1.00 *m* HCO_2H at 310 °C under 275 bar in two 316 SS cells (hereafter called 316 SSa and 316 SSb), the Pt/Ir alloy cell, and the Ti cell. Data from the 304 SS cell are not shown because, unlike the other materials, this cell was severely corroded by HCO_2H and quickly developed a leak. The inset in Figure 2 is an expansion of the 0−7 s region showing that small differences exist for the 316 SS and Pt/Ir cells in the early stage.

Two major features are apparent in Figure 2. First, the rate of CO_2 formation is markedly retarded in the Ti cell. We considered the possibility that CO_2 could migrate into the TiO_2 surface layer on Ti by the formation of $Ti(CO_3)_2$. There was no evidence that this took place in the form of surface corrosion. Moreover, all of the CO_2 was instantly flushed from the cell by pure H_2O as opposed to displaying a more gradual decrease that would be expected from shifting of the $Ti(CO_3)_2 \rightleftharpoons TiO_2 + 2CO_2$ equilibrium. It should be noted that welded Ti parts could not be used in this work because they were found to be rapidly corroded by CO_2-H_2O at 300 °C, perhaps because of the forementioned equilibrium.

A second major difference in Figure 2 is the different behavior of the CO_2 formation rate observed with 316 SSa[33] and 316 SSb. Initially, CO_2 is produced at about the same rate in both cells. Figure 3 shows, however, that a reproducible quiescent stage developed in the 316 SSa cell followed by an "explosive" stage. Considerable data scatter occurred in the explosive stage, suggesting that the reaction is not well controlled by the reactor. These cells were constructed from different lots of 316 SS, although both lots were found to have the same elemental

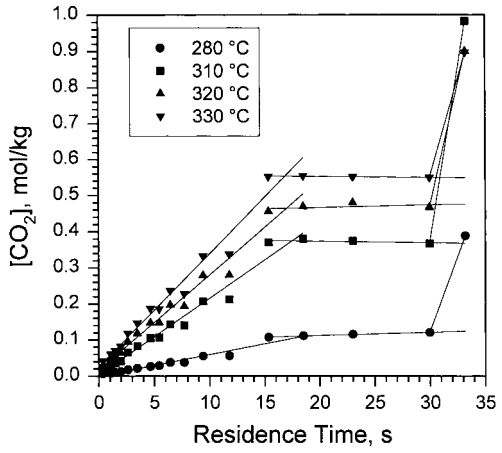

Figure 3. CO_2 concentration profiles from 1.00 *m* HCO_2H in the 316 SSa cell under 275 bar pressure showing anomalous but reproducible behavior.

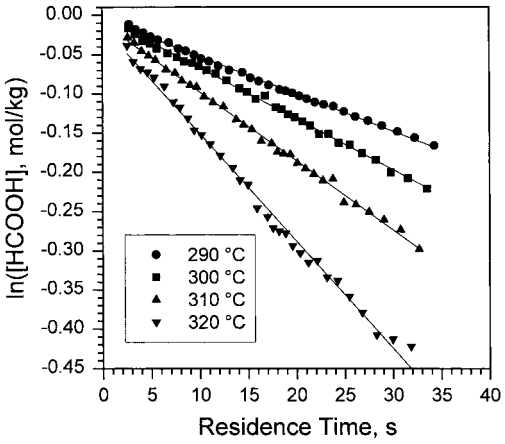

Figure 4. First-order rate plots for decarboxylation of 1.00 *m* HCO_2H at 275 bar in the 316 SSb cell.

TABLE 1: First-Order Rate Constants for Decarboxylation of 1.00 *m* HCO_2H (k_1) and HCO_2Na (k_2) under 275 bar[c]

cell type	*T*, °C	k_1, s^{-1} ($\times 10^3$)	k_2, s^{-1} ($\times 10^3$)
316 SSa[a]	280	5.9 ± 0.8	3.2 ± 0.3
	290	12.3 ± 1.6	4.7 ± 0.5
	310	25.7 ± 3.6	9.9 ± 1.9
	320	38.5 ± 6.3	13.7 ± 1.9
	330	46.0 ± 7.5	19.5 ± 1.9
316 SSb	290	7.7 ± 0.1	4.6 ± 0.3
	300	10.5 ± 0.1	5.7 ± 0.3
	310	14.7 ± 0.1	
	320	25.0 ± 0.4	
Pt/Ir	300	11.0 ± 0.8	13.8 ± 0.7
	310	20.7 ± 1.3	15.0 ± 1.1
	320	34.6 ± 0.8	17.8 ± 2.2
	330	44.7 ± 1.3	
Ti	290	1.8 ± 0.1	*b*
	300	2.8 ± 0.3	
	310	3.5 ± 0.1	
	320	3.9 ± 0.4	

[a] Initial stage before the quiescent stage (see Figure 2). [b] Rate was too slow to be measured on the time scale of the experiment. [c] Errors are standard deviations at 90% confidence interval.

TABLE 2: Arrhenius Parameters for Decarboxylation of 1.00 *m* HCO_2H and HCO_2Na, and 1.07 *m* Malonic Acid[a]

	HCO_2H		HCO_2Na		$HO_2CCH_2CO_2H$		$HO_2CCH_2CO_2Na$	
cell type	E_a, kJ/mol	ln(A, s^{-1})	E_a, kJ/mol	ln(A, s^{-1})	E_a, kJ/mol	ln(A, s^{-1})	E_a, kJ/mol	ln(A, s^{-1})
316 SSa	113 ± 10	19.6 ± 2.2	100 ± 1	16.1 ± 0.2	98 ± 5	24.0 ± 1.3	117 ± 5	28.3 ± 1.5
316 SSb	107 ± 12	17.9 ± 2.6			90 ± 31	21.4 ± 7.9		
Pt/Ir	120 ± 23	21.0 ± 4.6	31.4 ± 7.5	2.3 ± 1.5	91.5 ± 5	21.7 ± 1.2		
Ti	82 ± 12	11.2 ± 2.4			93 ± 8	21.4 ± 2.1		

[a] Errors are at 90% confidence interval.

composition by ICP-MS. They had a somewhat different usage history but no different from any of the other compounds we have studied where reproducible results have been obtained.[33−39,48,49] We searched unsuccessfully for several years to explain the unusual behavior of the 316 SSa cell but feel obliged to report the results. It is interesting to note that the behavior of 316 SSa is similar to the pattern of CO_2 production at 50−125 °C when formic acid is adsorbed on a clean Ni-(110) at about 10^{-10} Torr.[14] The explanation at these ultrahigh vacuum (UHV) conditions is that the initial first-order stage results from normal catalytic decomposition of HCO_2H on a metal surface.[12] As effective complete coverage of the surface by formate develops, the HCO_2^- ions impede decomposition of one another and the CO_2 production rate is slowed. This event is responsible for the quiescent period. The "explosive" stage results when "islands" of bare metal appear and catalyze the reaction very rapidly. There is no evidence of a formic anhydride intermediate.[50] It would be amazing if the same mechanism were to apply also to the surface exposed to fluid H_2O at high pressure and temperature, but the CO_2 production profile is similar. Although the surfaces of the 316 SSa and 316 SSb cells were not visually different after usage, a feature of decarboxylation of HCO_2H that differs from other acids studied in our work is the production of H_2. Possibly diffusion of H_2 through the steel surface is a factor. The 304 SS cell was severely corroded by HCO_2H but not by malonic acid, which liberates no H_2 upon decarboxylation.

Figure 2 does not prove that reaction 1 is solely wall-catalyzed and does not occur homogeneously. Rather, Figure 2 indicates that the decomposition of HCO_2H as measured by the formation of CO_2 is affected by the metal surface. In fact, the global rate of decomposition is likely to be a mixture of wall-catalyzed and homogeneous (perhaps H_2O-catalyzed) rates. In the present study, wall catalysis is a major factor. Another indication about the process comes from the determination of the kinetic constants, which is discussed next.

Kinetic constants were extracted from the rate of formation of CO_2 at ≤40% conversion. This condition enables a plug−flow model of the reactor to be used.[35,51] Because of the use of relatively low extents of conversion, however, the order of the process is not firmly established. Indeed, zeroth-, first-, and second-order rate plots for decomposition of HCO_2H and HCO_2Na were all found to be relatively linear. First-order behavior has been indicated previously for the decomposition of HCO_2H in H_2O,[11] as well as for acetic acid,[52] and will, therefore, be adopted.

A conventional first-order kinetic analysis by eq 7 affords k_1 of reaction 5.

$$-k_1 t = \ln\left[1 - \frac{[CO_2]_t - [HCO_2^-]_0[1 - \exp(-k_2 t)}{[HCO_2H]_0}\right] \quad (7)$$

In reality, this reaction is probably better described as pseudo-first-order because of the probable role of H_2O in the transition state. In eq 7, $[CO_2]$ was determined experimentally at various residence times (t); $[HCO_2^-]$ (0.19% at 290 °C, 0.09% at 330 °C) was obtained by an iso-Coulombic fit of the dissociation constant of HCO_2H,[53,54] and k_2 was determined from parallel experiments on the decarboxylation of 1.00 *m* HCO_2Na. The same procedure was used to study HCO_2Na as was used for HCO_2H except that its decarboxylation rate was too slow to measure in the Ti cell. Figure 4 is a first-order rate plot for the disappearance of HCO_2H constructed from eq 7 at several temperatures in the 316 SSb cell. Table 1 summarizes k_1 and k_2 as a function of temperature and cell type. The statistical analysis procedure was described in the Experimental Section.

It is noteworthy that the rate of decarboxylation of HCO_2Na (eq 6) in Table 1 is slower than that of HCO_2H (eq 5). The only exception is the rate in the Pt/Ir cell below 305 °C. Otherwise, the general trend of $k_1 > k_2$ is in line with findings for malonic acid[38] and acetic acid[52] and may be attributed to the additional resonance stabilization energy in the anion.

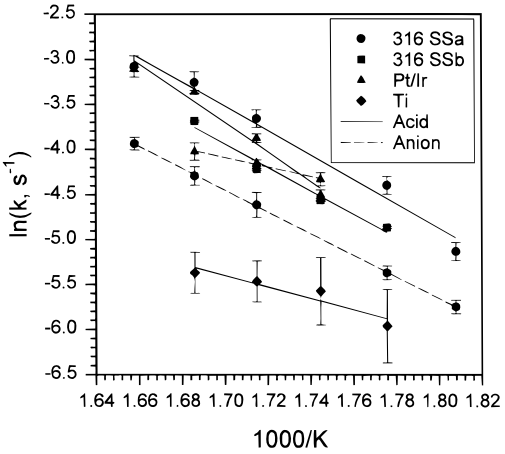

Figure 5. Arrhenius plots for hydrothermal decarboxylation of HCO_2H and HCO_2Na (eqs 5 and 6) in cells of the same design but different materials of construction. The Arrhenius constants are given in Table 2.

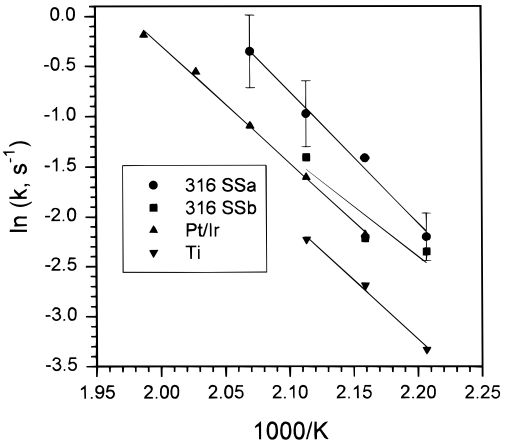

Figure 6. Arrhenius plots for hydrothermal decarboxylation of malonic acid ($HO_2CCH_2CO_2H$) at 275 bar in the same cells used for HCO_2H (see Figure 5). Table 2 gives the Arrhenius parameters.

The rate constants in Table 1 afford the Arrhenius plots shown in Figure 5. Table 2 contains the Arrhenius constants obtained by weighted least-squares regressions. E_a and ln A for decarboxylation of HCO_2H in Pt/Ir and the initial stage in the SS cells are the same within the experimental error. On the other hand, those for HCO_2H in Ti are statistically different. Likewise, the Arrhenius parameters for HCO_2Na are different or close to being statistically different from those of HCO_2H. The general range of E_a values of 83−121 kJ/mol for HCO_2H resembles the surface-catalyzed values of 100−109 kJ/mol,[14,21] and 86−113 kJ/mol when HCO_2H is decomposed in the presence of H_2O.[22,23] The range of E_a in Table 2 also includes the calculated value of 90 kJ/mol when two units of H_2O are incorporated in the transition state to catalyze the decarboxylation reaction.[8] These E_a values are much lower than those found for unimolecular decomposition, which are reportedly greater than 200 kJ/mol[25] and more typically greater than 250 kJ/mol.[8,26,29] Hence, the Arrhenius parameters for HCO_2H in the hydrothermal medium are consistent with some form of catalyzed decarboxylation.

A third comparison of data that support the contribution of wall catalysis in the decarboxylation of HCO_2H is with the corresponding Arrhenius constants for decarboxylation of malonic acid by eq 8. In contrast to monocarboxylic acids, dicarboxylic acids have been suggested to decarboxylate mainly without catalysis.[55] Hence, the rates of

$$HO_2CCH_2CO_2H \rightarrow CH_3CO_2H + CO_2 \qquad (8)$$

decarboxylation of malonic acid should be independent of the materials used to construct the cell. Although most of the experimental data for malonic acid in Table 2 were reported before,[38] a less sophisticated statistical analysis was used previously, which affects the Arrhenius parameters. The values in Table 2 were recalculated using the same procedure employed for formic acid. Figure 6 shows the resulting Arrhenius plots for malonic acid in the same cells used to study formic acid. Although small differences exist in the rates, the Arrhenius parameters lie within the uncertainty limits. The first-order rate of decomposition is, however, much faster than that of formic acid because of the higher preexponential factor and the slightly lower average values of the activation energy. Unlike formic acid, whose decarboxylation reaction appears to be catalyzed by H_2O and/or the reactor wall, malonic acid can form an internal, six-membered, cyclic transition state and thereby decarboxylate unimolecularly.[38,55] We have also investigated the decarboxylation of five additional monocarboxylic acids in the SS and Ti cells and find that the rates are essentially the same in these two materials of construction.[56]

In summary, the dependence of reaction 1 on the metal used in cell construction, the magnitude of its activation energy, and the comparison with noncatalyzed decarboxylation of malonic acid all suggest that decarboxylation of HCO_2H is catalyzed in these experiments. It is logical that catalysis in the hydrothermal medium involves both H_2O and the reactor wall in a ratio that varies with the material of construction, S/V, and perhaps the pressure and temperature. Unfortunately, experimental limitations at hydrothermal conditions make it difficult to probe the mechanism of surface catalysis further, but plans are underway in our laboratory to gain more fundamental insight into catalyzed reactions in the hydrothermal medium.

Acknowledgment. We are grateful to the U.S. Army Research Office for support of this work on DAAL03-92-G-0174 (R. W. Shaw, program manager).

References and Notes

(1) Klatt, M.; Röhrig, M.; Wagner, H. Gg. *Z. Naturforsch.* **1992**, *47A*, 1138.
(2) Ross, D. S.; Hum, G. P.; Miin, T.; Green, T. K.; Mansami, R. In *Supercritical Fluids—Chemical and Engineering Principles and Applications*; Squires, T. G., Paulaitis, M. F., Eds.; *ACS Symposium Series 339*; American Chemical Society: Washington, DC, 1987; p 242.
(3) Penninger, J. M. L. *Fuel* **1989**, *68*, 983.
(4) Margolis, L. Ya. *J. Catal.* **1971**, *21*, 93.
(5) Elliott, D. C.; Hallen, R. T.; Sealock, L. J., Jr. *Ind. Eng. Chem. Prod. Res. Dev.* **1983**, *22*, 431.
(6) Helling, R. K.; Tester, J. W. *Energy Fuels* **1987**, *1*, 417.
(7) Helling, R. K.; Tester, J. W. *Environ. Sci. Technol.* **1988**, *22*, 1319.
(8) Melius, C. F.; Bergan, N. E.; Shepherd, J. E. *Twenty-Third Symposium (International) on Combustion*; The Combustion Institute: Pittsburgh, PA, 1990; p 217.
(9) Hirth, Th.; Franck, E. U. *Ber. Bunsen-Ges. Phys. Chem.* **1993**, *97*, 1091.
(10) Rice, S. F.; Steeper, R. R.; Aiken, J. D. *J. Phys. Chem.*, in press.
(11) Bjerre, A. B.; Sorensen, E. *Ind. Eng. Chem. Res.* **1992**, *31*, 1574.
(12) Trillo, J. M.; Munuera, G.; Criado, J. M. *Catal. Rev.* **1972**, *7*, 51.
(13) McCarty, J.; Falconer, J.; Madix, R. J. *J. Catal.* **1973**, *30*, 235.
(14) Falconer, J.; Madix, R. J. *Surf. Sci.* **1974**, *46*, 473.
(15) Benziger, J. B.; Madix, R. J. *Surf. Sci.* **1979**, *79*, 394.
(16) Barteau, M. A.; Bowker, M.; Madix, R. J. *Surf. Sci.* **1980**, *94*, 303.
(17) Benziger, J. B.; Schoofs, G. R. *J. Phys. Chem.* **1984**, *88*, 4439.
(18) Shustorovich, E.; Bell, A. T. *Surf. Sci.* **1989**, *222*, 371.
(19) Sekine, I.; Senoo, K. *Corros. Sci.* **1984**, *24*, 439.
(20) Sekine, I.; Hatakeyama, S.; Nakazawa, Y. *Corros. Sci.* **1987**, *27*, 275.
(21) Giner, J.; Rissmann, E. *J. Catal.* **1967**, *9*, 115.
(22) Barham, H. N.; Clark, L. W. *J. Am. Chem. Soc.* **1951**, *73*, 4638.
(23) Yu, J.; Savage, P. E. *Ind. Eng. Chem. Res.* **1998**, *37*, 2.
(24) Blake, P. G.; Hinshelwood, C. *Proc. R. Soc. London, Ser. A* **1960**, *255*, 444.
(25) Blake, P. G.; Davies, H. H.; Jackson, G. E. *J. Chem. Soc. B* **1971**, 1923.
(26) Saito, K.; Kakumoto, T.; Kuroda, H.; Torii, S.; Imamura, A. *J. Chem. Phys.* **1984**, *80*, 4989.
(27) Ruelle, P.; Kesselring, U. W.; Nam-Tran, H. *J. Am. Chem. Soc.* **1986**, *108*, 371.
(28) Goddard, J. D.; Yamaguchi, Y.; Schaefer, H. F., III. *J. Chem. Phys.* **1992**, *96*, 1158.
(29) Francisco, J. S. *J. Chem. Phys.* **1992**, *96*, 1167.
(30) Hsu, D. S. Y.; Shank, W. M.; Blackburn, M.; Lin, M. C. *Nineteenth Symposium (International) on Combustion*; The Combustion Institute: Pittsburgh, PA, 1983; p 89.
(31) Ramsonov, F. N.; Petrov, A. K.; Baklanov, A. V.; Vihzin, V. V. *React. Kinet. Catal. Lett.* **1976**, *5*, 197.
(32) Akiya, N.; Savage, P. E. *AIChE J.* **1998**, *44*, 405.
(33) Brill, T. B.; Schoppelrei, J. W.; Maiella, P. G.; Kieke, M. L.; Belsky, A. J. *Proceedings of the 2nd International Conference on Solvothermal Reactions*; Committee of Solvothermal Technology Research: Takamatsu, Japan, 1996; 5.
(34) Kieke, M. L.; Schoppelrei, J. W.; Brill, T. B. *J. Phys. Chem.* **1996**, *100*, 7455.
(35) Schoppelrei, J. W.; Kieke, M. L.; Wang, X.; Klein, M. T.; Brill, T. B. *J. Phys. Chem.* **1996**, *100*, 14343.
(36) Schoppelrei, J. W.; Kieke, M. L.; Brill, T. B. *J. Phys. Chem.* **1996**, *100*, 7463.
(37) Belsky, A. J.; Brill, T. B. *J. Phys. Chem. A* **1998**, *102*, 4509.
(38) Maiella, P. G.; Brill, T. B. *J. Phys. Chem.* **1996**, *100*, 14352.
(39) Lundegard, P. D.; Kharaka, Y. K. *ACS Symposium Series*; American Chemical Society: Washington, DC.; 1990; Vol. 416, p 169.
(40) Shock, E. L. *Geochim. Cosmochim. Acta* **1993**, *97*, 3341.
(41) Katritzky, A. R.; Allin, S. M.; Siskin, M. *Acc. Chem. Res.* **1996**, *29*, 399.
(42) Savage, P. E.; Gopalan, S.; Mizan, T. I.; Martino, C. J.; Brock, E. E. *AIChE J.* **1995**, *41*, 1723.
(43) Tester, J. W.; Holgate, H. R.; Armellini, F. J.; Webley, P. A.; Killilea, W. R.; Hong, G. T.; Barner, H. E. *ACS Symposium Series*; American Chemical Society: Washington, DC, 1993; Vol. 518, p 35.
(44) Ding, Z. Y.; Frisch, M. A.; Li, L.; Gloyna, E. F. *Ind. Eng. Chem. Res.* **1996**, *35*, 3257.
(45) Maiella, P. G.; Brill, T. B. To be published.
(46) Cvetanoric, R. J.; Singleton, D. L. *Int. J. Chem. Kinet.* **1977**, *9*, 481.
(47) Reva, I. D.; Plokhotnichenko, A. M.; Radchenko, E. D.; Sheina, G. G.; Blagoi, Yu. P. *Spectrochim. Acta* **1994**, *50A*, 1107.
(48) Schoppelrei, J. W.; Brill, T. B. *J. Phys. Chem. A.* **1997**, *101*, 2298.

(49) Schoppelrei, J. W.; Brill, T. B. *J. Phys. Chem. A.* **1997**, *101*, 8593.
(50) Avery, N. R.; Toby, B. H.; Anton, A. B.; Weinberg, W. H. *Surf. Sci.* **1982**, *122*, L574.
(51) Cutler, A. H.; Antal, M. J., Jr.; Jones, M., Jr. *Ind. Eng. Chem. Res.* **1988**, *27*, 691.
(52) Bell, J. L. S.; Palmer, D. A.; Barnes, H. L.; Drummond, S. E. *Geochim. Cosmochim. Acta* **1994**, *58*, 4155.
(53) Kortum, G.; Vogel, W.; Andrussow, K. *Dissociation Constants of Organic Acids in Aqueous Solutions*; Butterworths: London, 1961.
(54) Bell, J. L. S.; Wesolowski, D. J.; Palmer, D. A. *J. Solution Chem.* **1993**, *22*, 125.
(55) Bell, J. L. S.; Palmer, D. A. In *Organic Acids in Geological Processes*; Pittman, E. D., Lewan, M. D., Eds.; Springer-Verlag: Heidelberg, 1994; p 226.
(56) Belsky, A. J.; Brill, T. B. To be published.